Chapter 9

DIRECT-IMAGING AND FREEZE-FRACTURE CRYO-TRANSMISSION ELECTRON MICROSCOPY OF MOLECULAR GELS

Dganit Danino[1] and Yeshayahu Talmon[2]
[1]*Department of Biotechnology and Food Engineering and*
[2]*Department of Chemical Engineering, Technion-Israel Institute of Technology, Haifa 32000, Israel*

1. Introduction 251
2. Cryo-TEM 252
3. Cryo-TEM Investigations of LMOG Gels 256
4. Conclusions and Perspectives for the Future 269

1. Introduction

Full characterization of liquid, semi-liquid, gel, or solid systems requires direct, supramolecular-level information (i.e., images, which show how molecules arrange to form clusters of various sizes and shapes). Cryogenic-temperature transmission electron microscopy (cryo-TEM) is the method of choice for obtaining such direct imaging of liquid or semi-liquid specimens, thermally fixed into a vitreous or quasi-solid state. Cryo-TEM provides high-resolution direct images of the assemblies in the system. Thus, it can elucidate the nature of the basic building blocks that make up the systems, covering a wide range of length scales from few nanometers to several microns. In addition, coexistence of many different assemblies present in the examined systems is quite easily observed in the micrographs. The interpretation of data cryo-TEM produces is usually quite straightforward, not model-dependent. In contrast, experimental interpretation data from "indirect methods", such as scattering techniques, is model dependent and is complicated when the system contains more than one type of aggregate or a broad size distribution.

R.G. Weiss and P. Terech (eds.),
Molecular Gels. Materials with Self-Assembled Fibrillar Networks, 251–272.

In the case of molecular gels, the unique rheological properties are the result of supramolecular aggregates. Those may be regular or irregular, homogenous or very diverse. Thus, cryo-TEM is most useful to image the range of the nanostructures present in those systems. In some cases, direct images provide the only way to prove a suggested or a theoretically predicted model. That was demonstrated for example in the case of the theoretically predicted branched micelles [1], the shape of the "end-caps" of thread-like micelles [2, 3], and the exact nanostructure and mechanism of formation of lithocholate nanotubes [4, 5].

While micrographs are most useful, at the same time one should keep in mind that cryo-TEM is not a strictly quantitative technique. It is the technique of choice to determine the structural building blocks of complex fluid systems, but the quantitative data should be usually provided by other techniques, such as small-angle X-ray scattering (SAXS) (see Chapter 11), small-angle neutron scattering (SANS) (see Chapter 10), or nuclear magnetic resonance (NMR). Another advantage of these scattering techniques is that they probe the bulk of the system, not just a small sample of it; they thus provide a real statistical average. However, in a very heterogeneous system, such an average may be difficult to interpret. In addition, these techniques are "model dependent"; they not "observer-dependent". In fact, the best experimental approach is to apply cryo-TEM to collect data on the nature of the nano-building blocks of the system, use that information to construct a physical model that is used to interpret data from the above mentioned "indirect techniques", and then check whether those latter results agree with cryo-TEM images to rule out possible artifacts.

Below we describe the basic aspects of cryo-TEM. That is followed by a review of the applications of the technique to the study of gel and gel-like systems. The interested reader will find more details about the technique and its application to other systems in references [6, 7].

2. Cryo-TEM

To examine samples that contain high concentrations of liquids in the TEM, it is necessary to lower in the vapor pressure to make them compatible with the high vacuum in the microscope column, lower typically than 10^{-6} Pa. Also, any supramolecular motion must be arrested to prevent blurring of the recorded image. TEM specimens must be thin, not thicker than about 300 nm. Thicker specimens give rise to inelastic electron scattering that deteriorates image quality. However, inelastically scattered electrons may be filtered out by electron microscopes equipped with an in-column or post-column energy filter.

We can reduce vapor pressure and arrest supramolecular motion by either "chemical" or "physical" (thermal) fixation. Chemical fixation involves addition of an alien chemical substance to the sample. Because microstructured

fluids are very sensitive to changes in composition, addition of compounds such as a stain or fixative, followed in some cases by a chemical reaction between the fixative and the specimen, and often by drying the sample, may alter the original microstructure of the studied system. That makes chemical fixation unacceptable for the study of microstructured fluids. Hence, the method of choice is thermal fixation (i.e., ultra-fast cooling of the liquid specimens into a vitrified or quasi-solid state). This is achieved by rapidly plunging the specimen into a suitable cryogen. Because thermal diffusivities are larger than mass diffusivities, thermal fixation is much more rapid than chemical fixation, and, of course, eliminates the addition of an alien compound to the system.

The cooling rate needed for vitrification of water is on the order of 100,000 K/s, as estimated theoretically [8] and measured experimentally in an actual specimen preparation set-up [9]. When cooling is too slow, hexagonal or cubic ice forms in aqueous systems, or other crystalline matrices may form in non-aqueous systems. Such crystalline matrix formation leads to optical artifacts, to mechanical damage to the microstructure, and to redistribution of solutes. Solutes are expelled from the growing ice lattice, and are deposited either in the crystal grains or often at grain boundaries.

The high cooling rates needed for vitrification require very large surface area-to-volume ratio. The geometry of choice is a thin film. Thin films (up to 300 nm thick, as stated above) are also required due to the limited penetration power of even high-energy electrons. High-resolution imaging requires thinner samples. It should be emphasized that most direct-imaging vitrified specimens display a wide thickness range. While microscopes operating at 200, 300 and 400 kV, found in many universities and research institutes, are capable of imaging specimens thicker than specified above, image interpretation becomes increasingly more difficult with specimen thickness. It is the high depth-of-focus of the TEM that leads to superposition of information from many layers of thick specimens, all projected on the plane of the detector.

The cryogen needed to successfully vitrify the specimen has to be at a low temperature, and well below its boiling point to avoid formation of a gas film around the specimen during quenching; such a gas film acts as a thermal insulator (the so-called Leidenfrost effect). The cryogen should also have a high thermal conductivity. Liquid nitrogen is a poor cryogen because of the narrow temperature range between its freezing and boiling. In contrast, liquid ethane, cooled to its freezing point (-183° C) by liquid nitrogen, is the best cryogen (its normal boiling point is about 100 K higher).

Another issue is the preservation of the nanostructure at precise conditions of (especially) temperature and concentration. This cannot be achieved unless the specimen is prepared in a controlled environment of the prescribed temperature and atmosphere that prevents loss of volatiles (e.g., water vapor) from the specimen during preparation. This requires a so-called controlled-environment vitrification system (CEVS). Several models are available, especially the relatively

simple but very reliable systems based on that developed by Bellare *et al.* [10] and modified by Talmon and co-workers over the years [9, 11], and the automatic "Vitrobot" of the FEI company that was developed by Frederik and co-workers [12]. The CEVS can be used from -10 to $+70^{\circ}$ C and with various saturated or unsaturated atmospheres.

Cryo-TEM specimen preparation is performed inside the CEVS, where the atmosphere is closed and controlled, from the outside. A small drop, typically 3 to 5 μL, of a pre-equilibrated system is pipetted onto a perforated carbon film supported on a TEM copper grid, held by tweezers and mounted on a spring-loaded plunger. The drop is blotted by filter paper wrapped on a metal strip, thus forming a thin liquid film supported on the perforated carbon film. After blotting, the plunging mechanism is activated, a trap door opens simultaneously, and the specimen is driven into the cryogen and vitrified. Finally, the vitrified sample is transferred under liquid nitrogen to the "working-station" of a cooling holder where it is loaded into the special holder and transferred in it into the microscope. In some cases, a "bare grid" (i.e., a microscope grid not covered by a perforated film) is used. More technical details can be found elsewhere [6, 10].

The blotting of the specimen may be performed in a number of ways. The simplest is wicking most of the liquid by simply touching the filter paper to the edge of the grid carrying the drop. Viscoelastic fluids require blotting with a shearing or "smearing" action. That temporarily reduces the viscosity of a shear-thinning liquid, allowing the formation of a thin enough liquid film on the support. Another way that can be performed either manually or, as in the case of the Vitrobot, automatically, is to press two pieces of blotting paper on the two sides of the specimen. That mode usually produces more uniform films. The blotting process and the confinement of the liquid in a thin specimen may introduce artifacts one should be aware of (see below). In addition to changes of the nature of the nanostructure, distortions of large objects, and alignment of slender "one dimensional" (rods or threads) or large "two-dimensional" (sheets) objects may take place.

While the prepared specimen is still in the liquid form, one can keep it in the controlled environment of the CEVS for some time. This allows the specimen to relax, following shear and elongation it may experience during blotting [13, 14], or to undergo other processes directly on-the-grid. Such processes may be chemical or physical reactions induced by different triggers, such as fast heating [9, 11] or cooling [15], pH jumps [16], or gelation. Those processes may be stopped at any intermediate stage by plunging the specimen into the cryogen. By repeating the experiment a number of times, each time allowing the process to proceed further towards completion, one can obtain a sequence of vitrified specimens that give "time-sectioning" of the process. This protocol is called "time-resolved cryo-TEM". Several variations of the CEVS have been built to facilitate such experiments [9, 11, 17].

On-the-grid cooling (or, in rare cases, heating) is a straightforward way to produce high-viscosity gel phases on the grid, starting with a low viscosity precursor. An example, described in some detail below, is that of a high viscosity lamellar phase formed upon cooling of a monoglyceride solution in olive oil. Above 50° C, the system is a low viscosity liquid which can be easily made into a thin liquid film in the properly controlled CEVS. The thin film is then cooled in the CEVS to about 40° C, and the formed gel is vitrified. In such cases one should use liquid nitrogen as the cryogen rather than liquid ethane, as the latter is a good solvent for many organic compounds even at its freezing point. Some systems, such as those containing glycerides, branched hydrocarbons or aromatics, do not crystallize readily upon cooling, and thus can be vitrified even in liquid nitrogen [18]. That is also true for aqueous systems containing sufficiently high concentrations of glycols (>20%) [14].

An indirect route to cryo-TEM is freeze-fracture-replication (FFR). This technique involves freezing the specimen (the specimen is larger than that of direct imaging cryo-TEM; thus in most cases vitrification is not accomplished), fracturing the frozen specimen, and preparing a metal replica of the fracture surface by vapor deposition. First, a heavy metal is deposited at an angle of 45° or less to the horizon, to enhance contrast ("shadowing"), and then a carbon layer is added for mechanical stability of the replica. Following replication, the sample is melted, the replica washed, dried, and imaged in the TEM at room temperature. The entire process of fracturing the specimen and replication is carried out in commercially available systems. Fast cooling may be carried out in the CEVS to allow quenching from given, well controlled, conditions [19]. FFR is most useful to examine high viscosity systems, or systems containing large particles that cannot be accommodated in the thin specimens of direct-imaging cryo-TEM; in both cases, direct-imaging cryo-TEM is not practicable. Of course, fine details or fine particles can be imaged by the technique. In fact, one early success in imaging a network structure of molecular organogel was achieved by applying the FFR technique in the study of a steroid/cyclohexane physical gel by Wade *et al*. [20]. While the technique is excellent to complement direct imaging cryo-TEM [4], it has lost popularity in the last two decades and, regrettably, is used in only a few research laboratories.

To prevent warming, which may lead to water crystallization and rearrangement of material, the vitrified specimens must be kept under liquid nitrogen until they are examined in the microscope. In typical cryo work, transfer of specimen into the microscope is carried out in a "cryo-holder", a special specimen holder that can be cooled by liquid nitrogen to −165° C or lower.

Low inherent contrast of cryo-specimens and their sensitivity to electron-beam radiation-damage make them difficult to image. One has to take these factors into account and optimize the conditions to extract as much information as possible from the specimen. For most applications, an acceleration voltage of 120 to 200 kV is used. The lower acceleration voltage offers better contrast,

while the higher affords better penetration power, and, in some cases, better resolution. Because the cryo-specimen is the coldest spot in the vacuum system and could collect contaminants by condensation, the vacuum system of the microscope must be very clean. An "anti-contaminator", a device made of large liquid nitrogen-cooled surfaces installed in the microscope column as close as possible above and below the specimen, must be used to trap molecules of residual volatiles, preventing them from condensing on the specimen. Images are recorded by cooled slow-scan CCD cameras. Such cameras offer easy use, with straightforward low-dose operation and immediate post-microscopy image processing. Such features are vital for the study of cryo-specimens. Low electron dose exposure, not more than 10 $e^-/Å^2$, and possibly lower, is applied to minimize electron-beam radiation damage. Phase contrast (equivalent in principle to phase-contrast light microscopy, namely converting phase differences to amplitude differences in image formation) is regularly applied to enhance contrast by defocusing of the microscope objective lens. This must be applied with care to avoid loss of resolution and introduction of imaging artifacts.

The complications induced by the low inherent contrast and sensitivity of most molecular assemblies to electron-beam radiation damage are demonstrated in Figure 1 of a cubic phase of Pluronic127TM (F-127). F-127 is a commercial triblock copolymer, poly(ethyleneoxide)-poly(propyleneoxide)-poly(ethyleneoxide) (PEO-PPO-PEO), that, at low polymer concentrations, forms spheroidal micelles, ∼8–9 nm in diameter, consisting of a bulky hydrated shell and a fairly dense core. As the concentration is increased (>12.5%) and the micellar volume fraction grows, the micelles close-pack into a body centered cubic lattice, and gel. In cryo-TEM images of a 15% F-127 sample, no microstructures or texture are observed at regular electron doses (∼10 $e^-/Å^2$) used in examination of cryo-TEM specimens because of the low inherent contrast of the PEO and PPO polymer units (Figure 1, region A). At twice the exposure, the fine texture of the ordered cubic phase emerges (Figure 1, region B). It was confirmed by a fast-Fourier transform (FFT) that was easily applied to the digitally-recorded image. A third exposure of the concentrated sample to the electron beam leads to bubbling and complete distortion of the structure, as seen in the lower right part of the image (region C).

3. Cryo-TEM Investigations of LMOG Gels

In the following sections, we review direct-imaging and FFR studies of various gels formed by self-assembly and interactions between synthetic and natural biopolymers, lipids, and surfactants, manifested, as described below, in rich morphology and structure. Cryo-TEM has not been used extensively yet to study strictly "LMOG gel" and SAFIN systems. However, we feel that

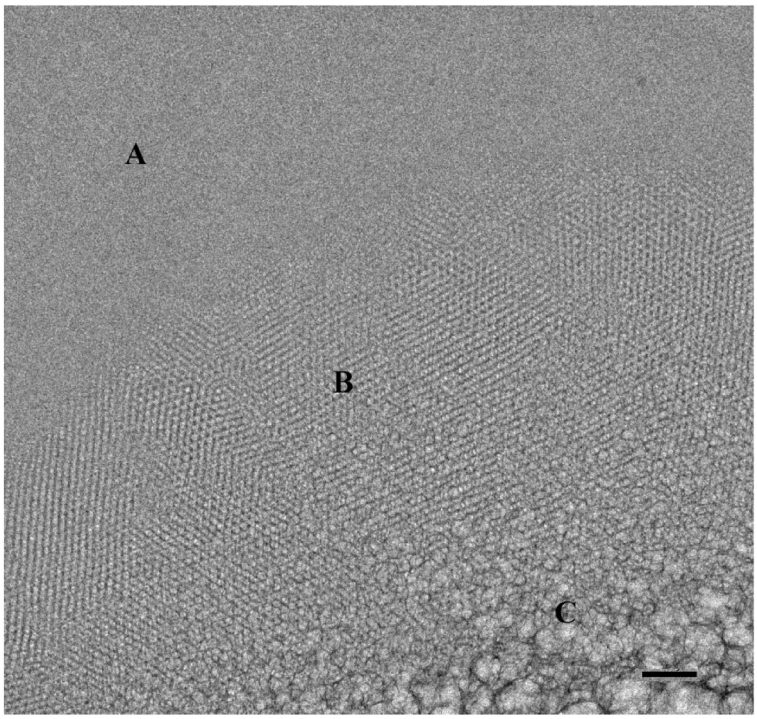

Figure 1. The effect of beam-exposure on the texture of low-contrast cubic mesophase of F-127. At low exposures of $\sim$10 $e^-/Å^2$, no texture is observed (region A). At twice this exposure, the fine texture of the ordered cubic phase appears (region B), and, at 3-times the electron dose, the structure is completely destroyed. Bar = 100 nm.

the examples shown here will be of interest to those who consider applying cryo-TEM. They illustrate potential applications of the technique, the difficulties associated with applying it to high-viscosity systems, and some routes to overcome those obstacles en route to successful direct imaging.

Freeze-fracture and direct-imaging cryo-TEM were used to study the viscous gel and diluted gel solutions of dioctadecyldimethylammonium chloride (DODMAC), which formed upon heating monohydrate crystal slurries to just below the Krafft temperature while stirring [21].

Typically, round liposomes and vesicles of up to several microns in diameter were observed in the diluted samples at 25° C, but some vesicles and small lens-like objects (suspended in solution or encapsulated in vesicles), with sharp corners or cusps, were also found (Figure 2A). Similar structures were seen in FF replicas of the viscous gel phase (Figure 2B). In contrast, mostly lens-like structures and multilamellar angular vesicles were found upon vitrification from 55° C, with a rather uniform spacing between membranes. Upon shearing at room temperature, mainly round and much smaller multilamellar vesicles

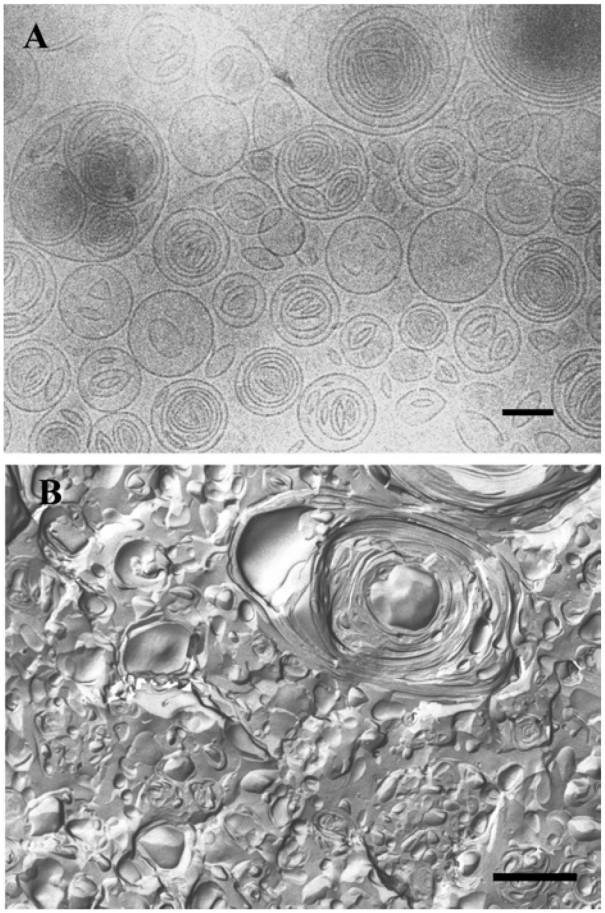

Figure 2. Cryo-TEM images of DODMAC dispersed in water: (A) direct-imaging micrograph of a 2% dispersion sheared at 50,000 s^{-1} to reduce vesicle size; (B) an FFR image of a 5% gel-like dispersion. Both images show the same building blocks, mainly multilamellar vesicles of a wide size-distribution, although the 2% solution flows freely while the 5% sample is in the gel phase. Bars = 100 nm.

were found, encapsulating both round and lens-shaped structures. The decrease in the vesicle size was coupled to a decrease in the viscosity. Upon aging, the vesicles collapsed to form a flat, layered structure, with an interlayer spacing of about 4 nm.

Vesicular phospholipid gels were also prepared by Kaiser and co-workers [22] for encapsulation and release of anticancer drugs. The gels were formed from mixtures of hydrogenated soy phoshpatidylcholine and cholesterol at different compositions by high-pressure homogenization. Small lens-like structures, similar to those seen in the DODMAC system, were found, free

in solution and entrapped within round vesicles. The membrane defects of the small, free lens-like structures (< 40 nm) were used to explain the fast initial drug release.

Maitra and co-workers [23] synthesized tripodal bile acid derivatives that act at low concentrations in the presence of organic cosolvents (such as acetone) to form transparent thermoreversible and thixotropic gels. Cryo-TEM images of the vitrified gel showed a well-developed intertwined network, made of very thin flat ribbons, 2 to 5 nm wide, that formed by one-dimensional growth of the tripodal bile. Twisted ribbons were also identified by cryo-TEM at the early stages of gel formation of hydrogelators of the bis-urea dicarboxylic acids family in the presence of $CaCl_2$ in Tris buffer [24]. The width of the ribbons ranged from 15 to 40 nm; the periodicity of the twisting was from 120 to 330 nm. The authors suggested that the ribbons are responsible for the gel formation, by becoming entangled, then trapping and immobilizing solvent via surface tension.

Viscoelastic solutions of lithocholic acid (LCA) form in an extended range of concentrations at basic pH. Helical ribbons and several microns long, stiff single-walled nanotubes, $\sim$52 nm in diameter and $\sim$1.5 nm thick, were identified by cryo-TEM in dilute LCA solutions [5]. Recently, FFR, direct-imaging cryo-TEM, and SAXS studies were performed to elucidate the early structures leading to the formation of the uniform tubes (Figure 3). Direct-imaging cryo-TEM images showed that less than 2 min after initiating the process by

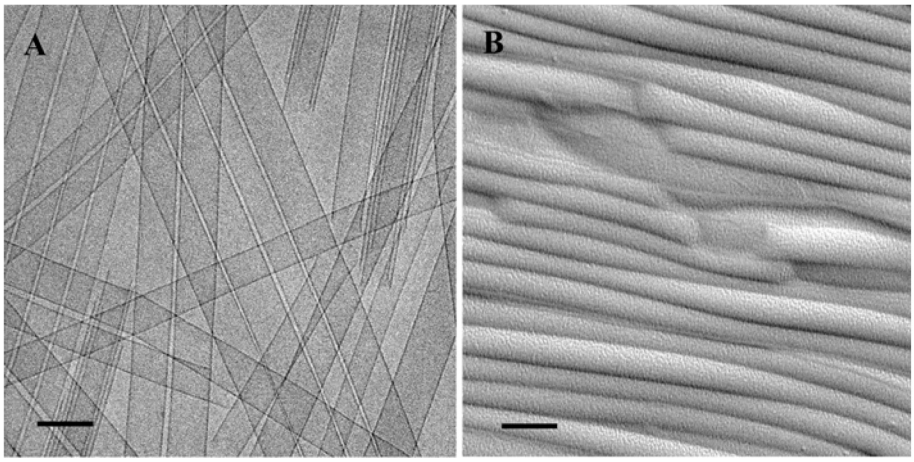

Figure 3. Direct-imaging and FFR images of LCA nanotubes. (A) 0.1% LCA in 0.05N NaOH, 6 min 50 s after mixing the components. Long, single- and multi-walled nanotubes are found at the early times of nanotubes formation. (B) 1% LCA in 0.1N NaOH, 6 days after mixing. Notice the similarity in dimensions (diameter and length) in the two images of the complementary cryo-TEM methods. Bars = 100 nm.

mixing LCA powder in aqueous NaOH solution, single- and multi-walled tubules of different diameters were formed [4]. Other intermediates, including helical ribbons and thin long fibers, were also observed within the first 30 min. The multi-wall structures were probably rather short-lived intermediates; after one hour they were no longer observed. Upon heating to 62° C, the tubes disintegrated and fibrillar aggregates, hundreds of micrometers long and resembling some of the intermediates found at the early times of the assembly, were found [25].

A comparative study on the assembly of the chiral amphiphile, N-dodecanoyl-(D- and L-) serine, under reversed polarity conditions was performed by Boettcher and co-workers [26]. Aqueous and toluene solutions were cooled from 110° C to room temperature to give gels, and then vitrified in liquid ethane and nitrogen, respectively. Multilamellar vesicles and tubules of about 1 mm in length, 80 nm in diameter, and inner channels of 25 nm, formed in toluene. Similar tubes but with diameters in the range of 80–139 nm were found in buffered solutions. Interestingly, the curvature did not change upon shifting from toluene to water, but much longer helices of up to 10 mm in length formed in water. In addition, many multilayered twisted ribbons of different widths were observed in water.

A gel-like phase consisting of microns long, overlapping, threadlike micelles was found during solubilization of small, unilamellar vesicles of phoshpatidylcholine-phosphatidic acid mixtures with the nonionic detergent dodecyl maltoside (DOM) [27]. Other intermediate structures observed during the solubilization process, prior to the micelles, include open and intact large unilamellar vesicles, and bilayer fragments. Upon solubilization of biological membranes (sarcoplasmic reticulum) by DOM, similar long micelles were seen, but they were less numerous and progressively broke down. In reconstitution studies by detergent removal, a slow transition through the gel-like phase led to the formation of multilamellar liposomes, while homogeneous unilamellar vesicles formed upon rapid transition. Another gel phase was identified upon addition of the bile salt, sodium desoxycholate (NaDOC), to cetyltrimethylammonium chloride (CTAB). This system has been studied by cryo-TEM, but the experiments were limited to the low viscosity conditions within the micellar phase [28]. Various structures were observed including mixed spheroidal micelles, flexible long and interconnected threadlike micelles, and short rodlike structures.

Schneider and co-workers [29], designed a 20-residue peptide that self-assembles in a pH-dependent manner to construct a chemically and mechanically responsive hydrogel. Intermolecular folding of this peptide into a β-hairpin is only permitted in basic aqueous solution (at pH $\geq$ 9), while acidification of the solution results in β-hairpin unfolding, and dissolution of the hydrogel. By cryo-TEM, they showed a network scaffold in the assembled conformation, which resembles the networks found in surfactant

systems. They also studied the gelation behavior of several amphiphilic diblock copolypeptides, 200 amino acids long, of which the poly(L-lysine) or poly (L-glutamic acid) hydrophilic block made up 80 or 90% of the structure, and the hydrophobic block was made of poly(L-leucine) or poly(L-valine). These copolypeptides form gels at low concentrations [30, 31]. The 90:10 mol% hydrophilic:hydrophobic group polypeptide was studied at concentrations up to 5 wt. %. Cryo-TEM images showed a gel scaffold consisting of interpenetrating membranous structures, several hundreds of nanometers long at all the concentrations studied. Within the cellular scaffold, particularly in the more diluted gels (1 and 2%), the lateral distances observed between neighboring cell membrane walls were larger than 100 nm [30]. In the case of the 80:20 polypeptide, a thin film of ~100 nm of the hydrogel was pre-formed, and then applied to the grid and vitrified. Cryo-TEM images showed the polypeptide gel was highly porous, made of membranous networks surrounded by significant amounts of water. Based on the appearance of the edges of the hydrogel matrix, it was concluded that the polypeptide associated throughout the sample until there was no free peptide in solution [31]. Hartgerink and co-workers, [32] designed a self-assembling peptide-amphiphile (PA) to prepare a nanostructured composite material that, upon mineralization, recreated the structural orientation between collagen and hydroxyapatite observed in bone. At low pH and concentrations above 2.5 mg/mL, PA formed birefringent gels in water which by cryo-TEM were shown to be a network of fibers about 7.6 nm in diameter and several microns in length.

The globular phosphoglycoprotein ovalbumin unfolds in solution upon heating. During unfolding, part of the hydrophobic regions are exposed, and denaturation is followed by aggregation, and, finally, gelation. At pH 7 and low ionic strength, ovalbumin self-organizes into linear cylindrical structures. The effect of electrostatic interactions on the gelation process at this pH was investigated by Weijers *et al*. [33], but with cryo-TEM they only studied the dilute solution. After heat treatment, long, flexible structures, about 5–7 nm in diameter and containing only very few branch points, were seen at low ionic strength. At higher ionic strength, but still below the gelation concentration, densely branched clusters were found. The authors concluded that the aggregation at this pH was essentially the same at different ionic strength, but branching is inhibited by electrostatic repulsions.

Gelation, precipitation, and re-dispersion may occur in mixed protein-surfactant systems. Khan and co-workers studied the gelation of a similarly charged system composed of lysozyme (a small ellipsoidal protein) and SDS (sodium dodecyl sulfate) [34]. In the absence of surfactant, small globular structures formed at low lysozyme concentrations. In the presence of low SDS concentrations, within the 3-phase region of precipitate, gel, and solution, short flexible aggregates, about 50 nm in diameter, were found to coexist with large sheet-like domains. A variety of other structures were identified at increasing

SDS concentrations near and after full redissolution of the precipitate, and at various total protein concentrations. Those structures included small globular assemblies and long rod-like (10 nm thick and 500–1500 nm long) intercrossing objects, termed star-like structures. No change in structures was observed upon aging for several weeks. Similar phase behavior, namely coexistence of precipitate, gel, and solution over a wide concentration range is exhibited by the system composed of oppositely charged ovalbumin and DOTAC (dodecyltrimethylammonium chloride) at pH above the isoelectric point [34]. In that system, flexible rod-like structures, which may constitute the gel phase, were identified. Sheet-like structures were not seen in the cryo-TEM images, but the authors found indications of large structures by light microscopy, suggesting the large objects may have been expelled from the cryo-TEM specimen during sample preparation (a known phenomenon in cryo-TEM). Similar structures were found in the transparent and bluish phases of the oppositely charged DOTAC-BSA (bovine serum albumin, prolate ellipsoidal structure) system. Neither precipitate nor gel was observed in that system up to very high protein concentrations.

Kappa-carrageenan (KC), a linear sulphated polysaccharide extracted form red algae, is often used in the food industry as a gelating agent. Thermoreversible gelation of KC occurs rapidly upon cooling, possibly as a result of a coil-to-double helix transition. KC may also be gelated isothermally (at constant ionic strength) by dialysis against "gel-inducing" salts such as KCl and CsCl [35]. Early cryo-TEM studies showed stiff microfibers several hundred in nm long and a few nm thick in the presence of KCl [36]. They were interpreted as individual KC helices. In a series of papers, Piculell and co-workers used the isothermal gelation approach to study the structure of intact and ultrasonically degraded KC in solution and towards the gel phase [37–39]. Using mixtures containing NaI and CsI salts at a constant salt concentration of 0.1M, they tuned the helix-helix interactions and the tendency of the helices to aggregate. Below CsI fractions of 0.4, no structures were observed. At higher concentrations where the viscosity increases, short and rigid "super-helical rods", $\sim$ 300–400 nm long and less than 5 nm thick, were found by cryo-TEM. Those structures, which were arranged in bundles of 2–8 fibers, aggregated into larger bundles and formed clusters and bigger aggregates as the amount of cesium salt was further increased [37, 39]. These findings indicated that the network formation occurs not through the double-helix formation itself, but only through association of helices. Additional experiments were conducted in the presence of locust bean gum (LBG), a plant polysaccharide having a random-coil structure in solution that considerably increases the gel strength of KC and reduces the minimum concentration for gelation. Cryo-TEM images showed thicker, polydispersed, and more flexible fibers in the presence of LBG, suggesting that LBG stabilizes the superhelical rods, and shifts the transition to a lower Cs content [38].

Amylose and amylopectin are the two main components of starch. Amylose is a linear polysaccharide, while amylopectin consists of short, highly branched amylose segments. Aqueous solutions of these two polysaccharides are unstable, and upon cooling or aging tend to gelate, precipitate, or crystallize, depending on their concentration and molecular weight. The mechanism of amylose gelation has been attributed to a transition from random coil configuration to a phase-separated gel-like network with polymer-rich and polymer-deficient regions. Cryo-TEM was used to characterize the behavior of dilute amylose and amylopectin aqueous solutions as a function of time, and to determine the dimensions and shape of the elementary structures constituting the networks at different steps of aggregation and crystallization [40]. Precipitation of amylose appeared as a continuous process involving network clustering of semicrystalline units of 10–15 nm in size into branched networks, followed by slow condensation of the networks into 300–500 nm domains, and later of thick semicrystalline aggregates, roughly composed of polygonal blocks. Amylopectin followed a similar pathway, and formed similar networks made of necklace-like substructures. However, those networks remained stable for several months and did not undergo further aggregation. It was suggested that long-range rearrangement of the crystallites into large aggregates was hindered by the branched configuration of the molecules.

Poly(ethylene glycol) (PEG) grafted with poly(lactic acid-co-glycolic acid), PEG-g-PLGA, was studied as a potential injectable drug delivery system. Low concentration aqueous solutions have low viscosity and flow freely at room temperature, but aqueous solutions with high concentrations of PEG-g-PLGA undergo a temperature dependent sol-to-gel transition [41]. In that study, the authors showed by cryo-TEM that micelles about 9 nm in diameter exist at low polymer concentrations and at 23.7° C.

Gels also formed upon absorption of PEG onto clay particles. At low polymer concentrations, aggregation was inhibited by steric interactions, while at high polymer and clay content the particles bridged to form gels. Recent cryo-TEM studies revealed the polymer-clay gels contain structures on multiple length-scales. Direct-imaging cryo-TEM of dilute pure clay solutions showed individual clay platelets, about 1 nm thick [42]. In the polymer-clay gel, characterized by FF, a fine texture of a network-like structure made of interconnected strings, ∼4 nm thick, was observed. These structures were interpreted as complexes consisting of the 1 nm clay objects with absorbed polymer layers of about 1.5 nm on each side, in agreement with values obtained from the dilute solutions and scattering data. Network formation was explained by bridging of neighboring clay particles by the polymer chains. These polymer-clay complexes extend to microns through formation of fibrous polymer-clay bundles, thus forming macroscopically homogeneous, transparent, shear-thinning hydrogels.

Paulsson and Edsman [43] studied the controlled-release of charged drugs from gels by adding surfactants that interact with both the drug and polymer

matrix. They investigated different types of gels, surfactants, and drugs, and characterized the drug-surfactant structures in polymer-free solutions and in gels by cryo-TEM. Unilamellar and oligolamellar vesicles, up to several hundred of nm in diameter, and open membranes, formed at physiological salt conditions in mixtures of oppositely charged diphenyldramine and SDS at a 1:2 drug:surfactant ratio. At half the SDS concentration, the system phase-separated, while at double the SDS content the viscosity increased, and long, highly branched threadlike micelles, similar to those found in surfactant/salt systems and forming a bicontinuous structure, were observed. Vesicles were found in mixtures of other drugs with SDS and negatively charged drugs with oppositely charged surfactants. Vesicles of similar sizes were also observed upon mixing 1:2 diphenyldramine and SDS in the gel, but they were facetted as a result of interactions with the polymer. Such vesicles were seen for the same solution composition of alprenolol and SDS, but, in the presence of the polymer C1342 (a covalently crossed-linked poly(acrylic acid) hydrogel with lipophilic modification), only very small vesicles, up to 50 nm in diameter, were found.

Mixtures of cationic polyelectrolytes and net negatively charged catanionic vesicles made of SDS and DDAB (didodecyldimethylammonium bromide) also show a wide region of phase separation containing solution and precipitate, and a polymer-rich gel region [44, 45]. Addition of JR-400 to the small catanionic vesicles within the bluish solution region resulted in the formation of huge concentric multilamellar vesicles coexisting with the small unilamellar and bilamellar vesicles. In the vicinity of the precipitation boundary facetted vesicles, open membranes, and disc-like aggregates became dominant, and then precipitation occurred. Addition of LM200 (a hydrophobically modified polymer) induced comparable changes, but at different ratios. Also, the variety of coexisting structures increased in the presence of LM200. Clustering of small vesicles suggested that the hydrophobic side chains of LM200, bearing the charge, anchor to the vesicle bilayer and cross-link them into possibly vesicle-polymer networks, though the polymer chains were not imaged. In the highly viscous polymer-rich phase and the gel phase, where excess of polymer charge existed, open bilayers and large membrane fragments, as well as disc-like structures that became dominant at higher polymer concentrations, were observed. Upon further addition of polymer, small elliptical vesicles reformed. Overall, an increase in the mean curvature was found with increase in the excess of polymer charge.

Mixing the oppositely charged surfactants, SDS and DOTAC, with the non-ionic hydrophobically modified hydroxyethyl cellulose (HMHEC) resulted in the formation of completely different structures [46]. Here, the viscosity increased with increasing DOTAC molar fraction at a constant polymer concentration, reflected structurally in a transition from spheroidal micelles to a structure of discrete micelles that were probably bound to (the invisible)

polymer organized in a repeating cell-like pattern, as shown by cryo-TEM. At high DOTAC concentrations, cell-like structures coexisting with unilamellar and multilamellar vesicles were seen by cryo-TEM; vesicles of up to several microns in diameter were detected by light microscopy.

While the polymer interacts with catanionic vesicles in the SDS/DDAB/JR-400 system discussed above, the interaction is between the polymer and a micelle-forming surfactant in SDS/JR-400 mixtures. Three distinct zones were identified with increase in the surfactant level, including a clear solution at low SDS concentrations and excess of polymer, precipitation and formation of a clear non-viscous solution and a gel-like phase around charge neutralization, and resolubilization at excess SDS, characterized also by a viscosity increase. In the presence of low SDS levels, mainly membranous structures were found, including bilayer fragments, small vesicles and disc-like aggregates [47]. Large aggregates of spheroidal and elongated micellar structures, disc-like structures, and a few vesicles were found in the turbid solution near the precipitation zone. At a 1:1 charge ratio, large globular and elongated flocs were found by both cryo-TEM and light microscopy. No structures were found in the supernatant at the precipitation zone (2:1 surfactant:polymer charge ratio), but a variety of structures were observed after resolubilization, including vesicles, disc-like and thread-like objects that possibly contributed to the increase in the viscosity. When resolubilization was completed, only spheroidal micelles were seen, probably free SDS micelles with only little interaction with the polymer, which was fully neutralized by SDS under those conditions.

In another anionic surfactant/cationic polyelectrolyte system, made of SDS and PDAC (poly(dialkyldimethylammonium chloride)), a variety of nano- and micro-particles were found upon changing the SDS/PDAC molar ratio [48]. Below the critical micellar aggregation of pure SDS in aqueous solutions, large domains of a well-ordered phase, with spacings of $\sim$4 nm, were found. Based on the images, and supported by SAXS data, the authors concluded that the ordered regions are of a hexagonal liquid crystalline phase of SDS that formed by screening of electrostatic interactions by the polymer charges. Small spheroidal micelles coexisting with particles of several tens on nm were observed in the solubilization domain. Many particles were facetted, with short threadlike micelles emerging from their surfaces. The size of these complexes decreased, and they became less numerous, as the solubilization process advanced by increasing the SDS/PDAC molar ratio, although complete solubilization was not reached and some (probably metastable) complexes coexisted with spheroidal micelles at all the conditions studied.

Viscous phases often form in surfactant solutions upon increasing the surfactant concentration or temperature, adding salt to charge surfactants, or varying the molar ratio between the components in mixed surfactant systems. In some cases, a sharp rise of several orders of magnitudes in the viscosity was reported, followed by a strong decrease to almost the viscosity of water [49, 50]; in a few

instances, the formation of a second viscosity peak was also found [49]. The viscosity increase was correlated to micellar growth, and the viscosity decrease was explained by a structural transition from linear to branched micelles and saturated networks [51]. These explanations are based primarily on the rheological measurements because direct structural information of such systems is still limited due to difficulties in preparing thin vitrified films of highly-viscous phases.

Early cryo-TEM studies by Clausen *et al*. [52] showed a transition from spheroidal to long, flexible micelles of cetyltrimethylammonium bromide and chloride surfactants at increasing salt concentration. More recently, Bernheim-Groswasser *et al*. [2] showed a gradual transformation from spheroidal micelles, existing at low surfactant concentrations, to long, threadlike micelles and then to elongated branched micelles and a saturated networks in aqueous solutions of the gemini (dimeric) surfactant, 12-2-12 (dimethylene-1,2-bis(dodecyl dimethylammonium bromide), at increasing concentrations. Vesicles were found in the viscous phase of the analogue hybrid fluorocarbon/hydrocarbon gemini surfactant $C_8^FC_4$-2-$C_8^FC_4$ [53], while saturated stiff networks were observed in the hybrid $C_8^FC_4$-2-12 dimer. It was further shown that after phase separation of $C_8^FC_4$-2-$C_8^FC_4$ and 12-2-12 mixtures, entangled threadlike micelles existed in the 12-2-12 rich phase (upper phase), while vesicles formed in the lower viscous phase contained mainly $C_8^FC_4$-2-$C_8^FC_4$. Other intermediates, including ribbons, open bilayers, small rings, and linear micelles, were observed depending on the mixing ratios between the various components [53].

Corce and co-workers [54] investigated the effect of added salt in the EHAC/KCl system, and correlated the microscopy findings to the rheological curve. Cryo-TEM images showed a transition from spheroidal micelles in the absence of salt to linear elongated micelles at low KCl concentrations (below the concentration of the viscosity peak), and to a network consisting of 3-fold junctions of branched micelles at compositions above the concentration of the viscosity peak. Linear and branched micelles were also shown by cryo-TEM in mixtures of $CpClO_3$/$NaClO_3$ (hexadecylpyridinium chlorate/sodium chlorate) [13]. However, folded and crumpled bilayer fragments were also found frequently in the vitrified samples. They were explained as long-lived intermediate structures that formed on the grid during specimen preparation by the strong shearing forces applied during blotting and formation of the thin films [13].

A peak in the viscosity vs. surfactant molar ratio curve was also reported for a system composed of the surfactant C12βG1 (*n*-dodecyl-β-D-glucopyranoside) in the presence of increasing SDS concentrations, above 40° C [55]. Our cryo-TEM studies [56] revealed a continuous transformation from a lamellar phase in the absence of SDS, through saturated micellar networks, to a micellar phase of spherical and short threadlike micelles, upon gradual

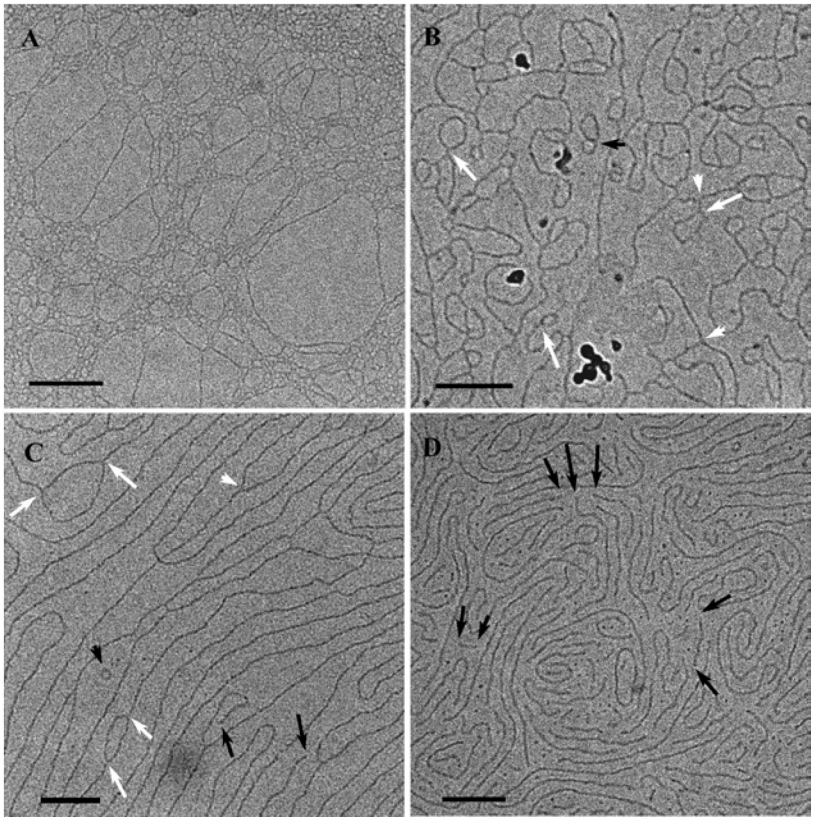

Figure 4. Cryo-TEM images of C12βG1/SDS mixtures, at a 5% constant total surfactant concentration and increasing SDS fractions equal to 0.07 (A), 0.14 (B) and 0.2 (C). Panels (A) and (B) relate to samples of comparable viscosity found below and above the viscosity peak concentration, respectively. Both images show well-developed networks made of elongated branched segments and closed rings. The network in (A) is saturated, while in (B) some free rings are also observed, but not micellar endcaps. At low viscosities ($\sim$0.01 Pa S, panel C) micellar endcaps appear, although interconnections between micelles are still frequent. (D) Threadlike and spheroidal micelles coexist at high SDS content. Arrowheads in B and C point to 3-fold junctions (white), and rings (black). Arrows point to micellar segments connected to rings (white), and micellar endcaps (black). Bars = 100 nm.

increase in SDS levels. In this system, however, saturated networks of different topology exist on both sides of the viscosity peak (Figure 4). At low SDS content, and throughout the region of concentrations below the viscosity peak, the network was made of multiple micellar segments that emerge typically from small, closely packed and connected rings (Figure 4A). At concentrations above the viscosity peak, where theoretically linear micelles should exist, a micellar phase of well-developed networks, consisting typically of 3-fold junctions, was found at high and medium viscosities. At high viscosities, the network was

saturated, while at medium viscosities individual rings were observed occasionally, coexisting with the connected micelles (Figure 4B). Upon further addition of charges, the number of junction points decreased and the number of micellar endcaps increased, but connected micelles were observed even at viscosities comparable to those of water (Figure 4C). Eventually, at much higher SDS content, linear thread-like assemblies formed and coexisted with globular micelles (Figure 4D).

Pure olive oil can be transformed into a butter-like spread (i.e., a "gel") by adding a sufficient amount of a monoglyceride. This is, of course, a phenomenon of interest to the food industry, and is behind the water-free olive-oil spread of the Eger Company of Israel. The product cannot be made into thin liquid films at room temperature and it melts into a low-viscosity liquid above 60° C. To directly image the nanostructure of this gel, we melted it at about 60° C, prepared cryo-specimens in a CEVS kept at the same temperature, cooled the grids to 58° C in the CEVS, and quenched the samples in liquid nitrogen. Olive oil is vitrified even in that rather poor cryogen. Figure 5 shows an example of such cryo-TEM images. Arrows point to stacks of lamellae. They have sufficient contrast only when positioned parallel to the electron beam. When they are positioned perpendicularly to the beam, there is insufficient contrast

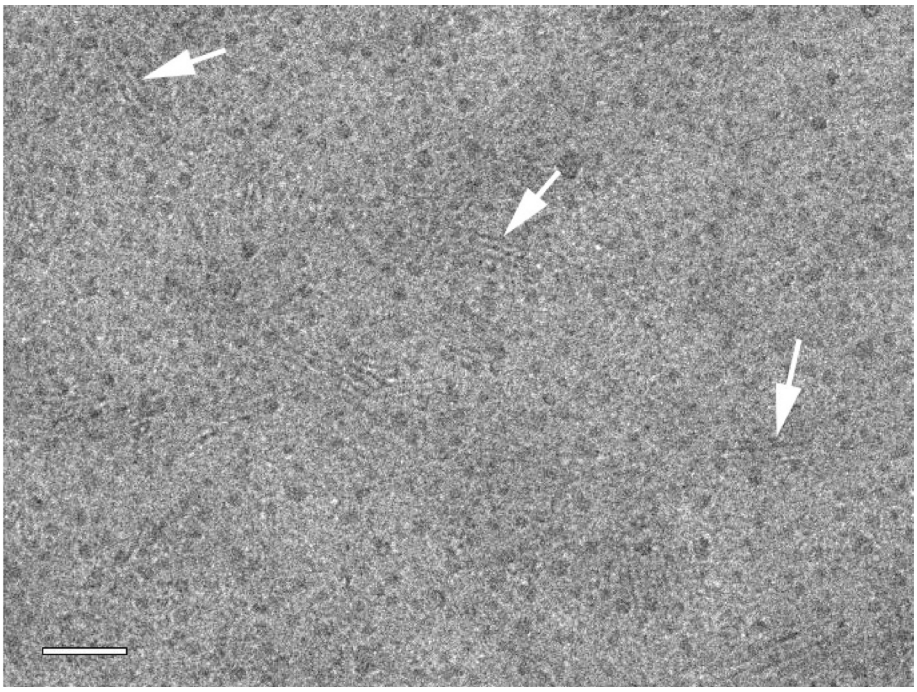

Figure 5. Cryo-TEM image of 7% monoglyceride in olive oil vitrified in the gel phase, from 58° C. Arrows point to stacks of lamellae that are parallel to the electron beam. Bar = 50 nm.

to make them visible; thus, much of the field-of-view does not show lamellae. That the gel phase is indeed made of small liquid crystalline domains was verified by SAXS and by light microscopy [15].

4. Conclusions and Perspectives for the Future

While the applications of direct imaging ("real-space") methods to elucidate the nanostructure of LMOG gels have been so far rather limited, recent technical development in cryo-TEM make the technique much more applicable for the study of those systems. Perhaps the most important development is the wide availability of reliable cooled-CCD cameras. Those cameras make low-dose imaging, vital for gel systems applications, much easier. Higher format cameras (4 mega-pixel, at least), and lower prices (they are still not cheap, but prices are expected to continue to fall) make them the tool of choice to record high resolution images that can be easily digitally processed. The great challenge when gels are concerned is still specimen preparation. We expect more on-the-grid gelation experiments to be used, applying either "home-built" or commercial CEVS-type systems. FFR, regrettably a "dying art", should be "revived" and used more for imaging high-viscosity systems.

Scanning probe microscopes, such as the atomic force microscope (AFM), are also potentially very useful. Many can be operated on liquid and semi-liquid systems under controlled temperature and humidity in operation modes that are minimally destructive to labile systems. Thus, we may expect to see clear images of gel systems emerge from these microscopes, too. A key to the success of this direction will depend on development of techniques by a "community" focusing on imaging this class of materials.

References

[1] Danino, D.; Talmon, Y.; Levy, H.; Beinert, G.; Zana, R.; "Branched thread-like micelles in an aqueous-solution of a trimeric surfactant", *Science*, **1995**, *269*, 1420–1421.

[2] Bernheim-Groswasser, A.; Zana, R.; Talmon, Y. "Sphere-to-cylinder transition in aqueous micellar solution of a dimeric (gemini) surfactant", *J. Phys. Chem. B*, **2000**, *104*, 4005–4009.

[3] Zheng, Y.; Won, Y.Y.; Bates, F.S.; Davis, H.T.; Scriven, L.E.; Talmon, Y. "Directly resolved core-corona structure of block copolymer micelles by cryo-transmission electron microscopy", *J. Phys. Chem. B*, **1999**, *103*, 10331–10334.

[4] Jean, B., Oss-Ronen, L.; Terech, P.; Talmon, Y. "Monodisperse bile salt nanotubes in water: kinetics of formation", *Adv. Mater.*, **2005**, *17*, 728–731.

[5] Terech, P.; de Geyer, A.; Struth, B.; Talmon, Y. "Self-assembled monodisperse steroid nanotubes in water", *Adv. Mater.*, **2002**, *14*, 495–498.

[6] Talmon, Y. "Cryogenic temperature transmission electron microscopy in the study of surfactant systems", In *Modern characterization methods of surfactant systems*, B.P. Binks, Ed., New York: Marcel Dekker, **1999**, Chap. 5, pp. 147–178.

[7] Danino, D.; Bernheim-Groswasser, A.; Talmon, Y. "Digital cryogenic transmission electron microscopy: an advanced tool for direct imaging of complex fluids", *Coll. Surf. A-Physicochem. Eng. Aspects*, **2001**, *183*, 113–122.
[8] Uhlmann, D.R. "A kinetic treatment of glass formation", *J. Non-cryst. Solids*, **1972**, *7*, 337–348.
[9] Siegel, D.P.; Green, W.J.; Talmon, Y. "The mechanism of lamellar-to-inverted hexagonal phase-transitions – a study using temperature-jump cryoelectron microscopy", *Biophys. J.*, **1994**, *66*, 402–414.
[10] Bellare, J.R.; Davis, H.T.; Scriven, L.E.; Talmon,Y. "Controlled environment vitrification system - an improved sample preparation technique", *J. Electron Microsc. Techn.*, **1988**, *10*, 87–111.
[11] Chestnut, M.H.; Siegel, D.P.; Burns, J.L.; Talmon, Y. "A temperature-jump device for time-resolved cryo-transmission electron-microscopy", *Microsc. Res. Techn.*, **1992**, *20*, 95–101.
[12] http://www.vitrobot.com/.
[13] Danino, D.; Talmon, Y.; Zana, R. "Cryo-TEM of thread-like micelles: on-the-grid microstructural transformations induced during specimen preparation", *Coll. Surf. A-Physicochem. Eng. Aspects*, **2000**, *169*, 67–73.
[14] Zheng, Y.; Lin, Z.; Zakin, J.L.; Talmon, Y.; Davis, H.T.; Scriven, L.E. "Cryo-TEM imaging the flow-induced transition from vesicles to threadlike micelles", *J. Phys. Chem. B*, **2000**, *104*, 5263–5271.
[15] Schmidt, J.; Eger, S.; Talmon, Y. (manuscript in preparation).
[16] Talmon, Y.; Burns, J.L.; Chestnut, M.H.; Siegel, D.P. "Time-resolved cryotransmission electron-microscopy", *J. Electron Microsc. Techn.*, **1990**, *14*, 6–12.
[17] Fink, Y.; Talmon, Y., "The Follow TEM Controlled Environment Vitrification System", In *Proc. 13th Int'l Congress on Electron Microsc.*, **1994**, *1*, p. 37.
[18] Danino, D.; Gupta, R.; Satyavolu, J.; Talmon, Y. "Direct cryogenic-temperature transmission electron microscopy imaging of phospholipid aggregates in soybean oil", *J. Coll. Interface Sci.*, **2002**, *249*, 180–186.
[19] Burns, J.L.; Talmon, Y. "Freeze-fracture-replication using the controlled environment vitrification system (CEVS)", *J. Electron Microsc. Techn.*, **1988**, *10*, 113–114.
[20] Wade, R.H.; Terech, P.; Hewat, E.A.; Ramasseul, R.; Volino, F. "The network structure of a steroid/cyclohexane physical gel", *J. Coll. Interface Sci.*, **1986**, *114*, 442–251.
[21] Laughlin, R.G.; Munyon, R.L.; Burns, J.L.; Coffindaffer,T.W.; Talmon, Y. "Physical science of the dioctadecyldimethylammonium chloride water-system .3. Colloidal aspects", *J. Phys. Chem.*, **1992**, *96*, 374–383.
[22] Kaiser, N.; Kimpfler, A.; Massing, U.; Burger, A.M.; Fiebig, H.H.; Brandl, M.; Schubert, R. "5-fluorouracil in vesicular phospholipid gels for anticancer treatment: entrapment and release properties", *Int. J. Pharm.*, **2003**, *256*, 123–1231.
[23] Mukhopadhyay, S.; Maitra, U.; Ira; Krishnamoorthy, G.; Schmidt, J.; Talmon, Y. "Structure and dynamics of a molecular hydrogel derived from a tripodal cholamide", *J. Am. Chem. Soc.*, **2004**, *126*, 15905–15914.
[24] Estroff, L.A.; Leiserowitz, L.; Addadi, L.; Weiner, S.; Hamilton, A.D.; "Characterization of an organic hydrogel: a cryo-transmission electron microscopy and X-ray diffraction study", *Adv. Mater.*, **2003**, *15*, 38–42.
[25] Oss-Ronen, L. "Nanoscopic characterization of self-assembled nanotubules of lithocholic acid in water", *Ms.C. Thesis, Technion – Israel Institute of Technology, Haifa, Israel*, **2004**.
[26] Boettcher, C.; Schade, B.; Fuhrhop, J.H. "Comparative cryo-electron microscopy of noncovalent N-dodecanoyl- (D- and L-) serine assemblies in vitreous toluene and water", *Langmuir*, **2001**, *17*, 873–877.

[27] Lambert, O.; Levy, D.; Ranck, J.L.; Leblanc, G.; Rigaud, J.L. "A new "gel-like" phase in dodecyl maltoside-lipid mixtures: implications in solubilization and reconstitution studies", *Biophys. J.*, **1998**, *74*, 918–930.

[28] Vethamuthu, M.S.; Almgren, M.; Brown, W.; Mukhtar, E. "Aggregate structure, gelling, and coacervation within the L(1) phase of the quasi-ternary system alkyltrimethylammonium bromide sodium deoxycholate water", *J. Coll. Interface Sci.*, **1995**, *174*, 461–479.

[29] Schneider, J.P.; Pochan, D.J.; Ozbas, B.; Rajagopal, K.; Pakstis, L.; Kretsinger, J. "Responsive hydrogels from the intramolecular folding and self-assembly of a designed peptide", *J. Am. Chem. Soc.*, **2002**, *124*, 15030–15037.

[30] Pochan, D.J.; Pakstis, L.; Ozbas, B.; Nowak, A.P.; Deming,T.J. "SANS and Cryo-TEM study of self-assembled diblock copolypeptide hydrogels with rich nano- through microscale morphology", *Macromolecules*, **2002**, *35*, 5358–5360.

[31] Pakstis, L.M.; Ozbas, B.; Hales, K.D.; Nowak, A.P.; Deming, T.J.; Pochan, D. "Effect of chemistry and morphology on the biofunctionality of self-assembling diblock copolypeptide hydrogels", *Biomacromolecules*, **2004**, *5*, 312–318.

[32] Hartgerink, J.D.; Beniash, E.; Stupp, S.I. "Self-assembly and mineralization of peptide-amphiphile nanofibers", *Science*, **2001**, *294*, 1684–1688.

[33] Weijers, M.; Visschers, R.W.; Nicolai, T. "Light scattering study of heat-induced aggregation and gelation of ovalbumin", *Macromolecules*, **2002**, *35*, 4753–4762.

[34] Moren, A.K.; Regev, O.; Khan, A. "A Cryo-TEM study of protein-surfactant gels and solutions", *J. Coll. Interface Sci.*, **2000**, *222*, 170–178.

[35] Viebke, C.; Borgstrom, J.; Piculell, L. "Characterization of kappa-carrageenan and iota-carrageenan coils and helices by malls/gpc", *Carbohydrate Polym.*, **1995**, *27*, 145–154.

[36] Sugiyama, J.; Rochas, C.; Turquois, T.; Taravel, F.; Chanzy, H. "Direct imaging of polysaccharide aggregates in frozen aqueous dilute systems", *Carbohydrate Polym.*, **1994**, *23*, 261–264.

[37] Borgstrom, J.; Piculell, L.; Viebke, C.; Talmon, Y. "On the structure of aggregated kappa-carrageenan helices. A study by Cryo-TEM, optical rotation and viscometry", *Int. J. Biol. Macromol.*, **1996**, *18*, 223–229.

[38] Chronakis, I.S.; Borgstrom, J.; Piculell, L. "Conformation and association of kappa-carrageenan in the presence of locust bean gum in mixed NaI/CsI solutions from rheology and cryo-TEM", *Int. J. Biol. Macromol.*, **1999**, *25*, 317–328.

[39] Piculell, L.; Borgstrom, J.; Chronakis, I.S.; Quist, P.O.; Viebke, C. "Organisation and association of kappa-carrageenan helices under different salt conditions", *Int. J. Biol. Macromol.*, **1997**, *21*, 141–153.

[40] Putaux, J.L.; Buleon, A.; Chanzy, H. "Network formation in dilute amylose and amylopectin studied by TEM", *Macromolecules*, **2000**, *33*, 6416–6422.

[41] Jeong, B.; Kibbey, M.R.; Birnbaum, J.C.; Won, Y.Y.; Gutowska, A. "Thermogelling biodegradable polymers with hydrophilic backbones: PEG-g-PLGA", *Macromolecules*, **2000**, *33*, 8317–8322.

[42] Loizou, E.; Butler, P.; Porcar, P.; Kesselman, E.; Talmon, Y.; Schmidt, G. "Large scale structures in nanocomposite hydrogels", (manuscript in preparation).

[43] Paulsson, M.; Edsman, K. "Controlled drug release from gels using surfactant aggregates. II. Vesicles formed from mixtures of amphiphilic drugs and oppositely charged surfactants", *Pharma. Res.*, **2001**, *18*, 1586–1592.

[44] Marques, E.F.; Regev, O.; Khan, A.; Miguel, M.D.; Lindman, B. "Interactions between catanionic vesicles and oppositely charged poly electrolytes-phase behavior and phase structure", *Macromolecules*, **1999**, *32*, 6626–6637.

[45] Regev, O.; Marques, E.F.; Khan, A. "Polymer-induced structural effects on catanionic vesicles: formation of facetted vesicles, disks, and cross-links", *Langmuir*, **1999**, *15*, 642–645.
[46] Nilsson, S.; Goldraich, M.; Lindman, B.; Talmon, Y. "Novel organized structures in mixtures of a hydrophobically modified polymer and two oppositely charged surfactants", *Langmuir*, **2000**, *16*, 6825–6832.
[47] Goldraich, M.; Schwartz, J.R.; Burns, J.L.; Talmon,Y. "Microstructures formed in a mixed system of a cationic polymer and an anionic surfactant", *Coll. Surf. A-Physicochem. Engin. Aspects*, **1997**, *125*, 231–244.
[48] Nizri, G.; Magdassi, G.; Schmidt, J.; Cohen, Y.; Talmon,Y. "Microstructural characterization of micro-and nanoparticles formed by polymer-surfactant interactions", *Langmuir* **2004**, *20*, 4380–4385.
[49] Hoffmann, H. "Viscoelastic surfactant solutions", In *Structure and Flow in Surfactant Solutions.*, ACS Symposium Series 578, C.A. Herb and R. K. Prud'homme, Eds., Washington, DC: The American Chemical Society, **1994**, Chap. 1, pp. 1–31.
[50] Raghavan, S.R.; Fritz, G.; Kaler, E.W. "Wormlike micelles formed by synergistic self-assembly in mixtures of anionic and cationic surfactants", *Langmuir*, **2002**, *18*, 3797–3803.
[51] Lequeux, F.; "Reptation of connected wormlike micelles", *Europhys. Lett.*, **1992**, *19*, 675–681.
[52] Clausen, T.M.; Vinson, P.K.; Minter, J.R.; Davis, H.T.; Talmon, Y.; Miller, W.G. "Viscoelastic micellar solutions - microscopy and rheology", *J. Phys. Chem.*, **1992**, *96*, 474–484.
[53] Oda, R.; Huc, I.; Danino, D.; Talmon, Y. "Aggregation properties and mixing behavior of hydrocarbon, fluorocarbon, and hybrid hydrocarbon-fluorocarbon cationic dimeric surfactants", *Langmuir*, **2000**, *16*, 9759–9769.
[54] Croce, V.; Cosgrove, T.; Maitland, G.; Hughes, T.; Karlsson, G. "Rheology, cryogenic transmission electron spectroscopy, and small-angle neutron scattering of highly viscoelastic wormlike micellar solutions", *Langmuir*, **2003**, *19*, pp. 8536–8541.
[55] Kaler, E.W.; Baser, B. (manuscript in preparation).
[56] Ziserman, L.; Baser, B.; Kaler, E.W.; Danino, D. (manuscript in preparation).